Silver Alloying in Highly Efficient CuGaSe 2 Solar Cells with Different Buffer Layers

Jan Keller, Lars Stolt, Tobias Törndahl, Marika Edoff

Solar RRL
www.solar-rrl.com

Silver Alloying in Highly Efficient $CuGaSe_2$ Solar Cells with Different Buffer Layers

Jan Keller, Lars Stolt, Tobias Törndahl, and Marika Edoff*

This study evaluates the effect of silver alloying, stoichiometry, and deposition temperature of wide-gap (Ag,Cu)$GaSe_2$ (ACGS) absorber films for solar cell applications. Devices using a standard CdS buffer exhibit a strong anticorrelation between the open-circuit voltage (V_{OC}) and short-circuit current density (J_{SC}), with V_{OC} decreasing and J_{SC} increasing toward stoichiometric absorber composition. Increasing the ACGS deposition temperature leads to larger grains and improved J_{SC}, while V_{OC} is not affected. By adding more silver to the absorber (maximum tested [Ag]/([Ag]+[Cu]) [AAC] = 0.4), the widening of the space charge region (SCR) significantly enhances carrier collection. Experimental quantum efficiency spectra can be accurately simulated when assuming a very low diffusion length and perfect collection in the SCR. The highest efficiency of 8.3% (without antireflection coating [ARC]) is reached for an absorber with AAC = 0.4 grown at 600 °C. Replacing CdS by a (Zn,Sn)O buffer with lower electron affinity strongly mitigates interface recombination. Moreover, the V_{OC}–J_{SC} anticorrelation is not evident anymore and the highest efficiency of 11.2% (11.6% w/ARC, V_{OC} = 985 mV, J_{SC} = 18.6 mA cm^{-2}, fill factor = 61.0%) is reached for a close-stoichiometric ACGS solar cell with AAC = 0.4 processed at 650 °C.

1. Introduction

The chalcopyrite semiconductor $CuGaSe_2$ exhibits a bandgap energy (E_G) of 1.6–1.7 eV[1–3] and is thus a promising absorber material for top solar cells in two-junction tandem devices.[4,5] However, the bulk quality of $CuGaSe_2$ is comparatively poor,[6,7] with a low electron lifetime resulting from a high Shockley–Read–Hall (SRH) recombination rate. Different origins, such as energetically deep defects (e.g., via Ga_{Cu}), a high density of defects, and/or detrimental, Cu-rich grain boundaries, are discussed.[8–16]

In addition to losses directly related to the $CuGaSe_2$ layer itself, front interface recombination is supposed to be pronounced when a standard CdS buffer is used. This is due to a negative conduction band offset (CBO) at the CdS/$CuGaSe_2$ interface ($\Delta E_C \approx -0.35$ eV), leading to a very minor (or absent) type inversion and a high recombination rate at the interface.[17–19]

The highest efficiencies of $CuGaSe_2$ solar cells reported so far are 11.9% for a sample with a $(Zn_{1-y},Sn_y)O_z$ (ZTO) buffer layer (our lab, noncertified)[2] and 11.0% with a standard CdS buffer layer (certified).[20] The corresponding photovoltaic parameters are open-circuit voltages (V_{OC}) of 1.017 and 0.901 V, short-circuit current densities (J_{SC}) of 17.5 and 17.1 mA cm^{-2}, and fill factors (FF) of 67.0 and 71.3%, respectively. Obviously, the main improvement when exchanging CdS by an alternative ZTO buffer layer is the higher V_{OC}, resulting from a reduced (or canceled out) interface recombination, as a negative CBO can be avoided when using ZTO.[21,22]

It has to be mentioned that in order to use these wide-gap devices in a tandem configuration, a transparent back contact (TBC) needs to be incorporated. So far, the highest efficiencies of $CuGaSe_2$ solar cells on TBCs are much lower, at about 5%.[23–26] Recently, research on the topic of TBCs has intensified and significant progress was observed, lifting the efficiency (η) of chalcopyrite solar cells with TBCs close to the level of those with standard Mo back contacts.[27–33] Thus, further improvements may be expected in the near future.

The best V_{OC} values for CdS-buffered samples are achieved after a postannealing at 200 °C, reaching 971 mV for a polycrystalline[34] and 946 mV for a single-crystal absorber.[35] However, usually the postannealing results in a decrease in FF and the best V_{OC} values for a sample without postannealing are about 920 mV[20,36] or 960 mV when a Cu-deficient surface layer was deliberately introduced and the CdS thickness increased.[37] In our lab, running a three-stage deposition process at a maximum temperature of 550 °C, the reported V_{OC} values for $CuGaSe_2$ cells with CdS buffer layers are typically in the range of 730–830 mV.[2,38,39] Differences in device parameters between research groups are explainable by details in the sample processing, such as the temperature,[2] metal evaporation profiles,[40] and Se flux[20] during absorber deposition, variations in the chemical bath deposition (CBD) protocol for CdS and its thickness,[36,37] and even different air exposure times (surface oxidation) before CBD.[40] Attempts to improve the

J. Keller, L. Stolt, T. Törndahl, M. Edoff
Ångström Solar Center
Division of Solar Cell Technology
Uppsala University
75121 Uppsala, Sweden
E-mail: jan.keller@angstrom.uu.se

The ORCID identification number(s) for the author(s) of this article can be found under https://doi.org/10.1002/solr.202300208.

DOI: 10.1002/solr.202300208

performance via the incorporation of heavy alkali elements, as observed in low-gap materials,[41] showed limited potential so far.[20,37]

It is suggested that Ag alloying, i.e., forming an (Ag,Cu)$GaSe_2$ (ACGS) compound, may mitigate recombination losses at the CdS/absorber interface because it increases the electron affinity and thus reduces the conduction band misalignment.[21,42,43] Indeed, higher V_{OC} values were reached for indium-containing, wide-gap Cu(In,Ga)Se_2 solar cells, when a substantial amount of silver was incorporated.[21,44–51] In addition, larger grains are typically observed with Ag alloying, due to a lower melting temperature[44] and enhanced reaction rates during the phase evolution.[52] This allows to significantly reduce the process temperature and thereby increasing the performance of solar cells with heat-sensitive polyimide substrates[53] and transparent back contacts.[27,54] It may be speculated that the larger grain size generally leads to a longer minority carrier diffusion length (L_n) when silver is incorporated. However, up to now, Ag alloying did not result in a significant improvement for pure $CuGaSe_2$ solar cells.[55]

In this contribution, the potential of silver addition in combination with the use of optimized ZTO buffer layers is studied. The aim is to significantly reduce the interface recombination and at the same time improving the absorber quality. First, the effects of absorber stoichiometry ([I]/[III] = I/III ≈ 0.7–1.2), silver content ([Ag]/[I] = AAC ≈ 0–0.4), and maximum deposition temperature (550 °C vs 600 °C) are studied on CdS-buffered samples. It is found that all resulting absorbers exhibit very similar band gap values of $E_G = 1.64 \pm 0.02$ eV, which allows a direct comparison between the effects of the different parameter variations. In the second part, different absorber compositions and metal ratios in ZTO (affecting its electron affinity[2,56,57]) were tested and the absorber deposition temperature was increased to 650 °C for all samples.

2. Results and Discussion

A three-stage coevaporation process was used to deposit the (A)CGS absorbers for all solar cells in this study, which characteristics are presented in the following. If not stated otherwise, the standard maximum temperature during the later part of the second and the whole third stage was 550 °C. Each run produced four different samples with individual absorber stoichiometry (i.e., I/III), but failed (e.g., peeled-off or shunted) samples were excluded (for more information, see ref. [48]). Only the best cell parameters (out of 14 cells) are shown for each sample for the sake of clarity and the trends of the average values are very comparable. All presented *I–V* curves in the article were (re-)measured after adjusting the illumination intensity to the $J_{SC,eqe}$ values, as calculated from the corresponding external quantum efficiency (EQE) spectra.

2.1. Effects of Absorber Stoichiometry, Growth Temperature, and Silver Addition

In this first part, only samples with CdS buffers are discussed and the effects of absorber stoichiometry, growth temperature, and silver content are evaluated.

It was shown that already small amounts of silver, added in the form of a thin precursor layer, can lead to a substantial performance boost in low-gap chalcopyrite solar cells.[27,54,58,59] Thus, in a first experiment, only copper, gallium, and selenium were coevaporated on Mo-coated glass substrates with (labeled "pre-Ag") or without a 10 nm-thick Ag precursor layer to produce (A)CGS solar cells. The application of the Ag precursor led to a rather low AAC of about 0.02 in the final absorber film.

Figure 1 exemplifies the effect on the cell performance and absorber morphology (samples from the same deposition run). It is evident that the carrier collection improves when Ag is added, expressed as higher EQE values in Figure 1a. The blue curve illustrates the "perfect EQE", excluding collection losses in the absorber and buffer layer. The curve was derived after measuring the 1) transmittance T_{abs} and reflectance R_{abs} of the bare absorber on a glass substrate, 2) total reflectance of the cell R_{cell}, and 3) absorptance of the window layer stack A_{win} on glass. The "perfect EQE" was then approximated by

$$\text{"Perfect EQE"} = (1 - R_{cell}) \times (1 - A_{win}) \times (1 - T_{abs}/(1 - R_{abs})) \quad (1)$$

The term $T_{abs}/(1 - R_{abs})$ follows from the correction of the measured transmittance. Due to an artificial and constant reduction of the measured T_{abs} for energies close to and below the absorber band gap energy (probably caused by light guiding through the edges of the glass substrate during the transmittance measurement), this procedure slightly overestimates the theoretically perfect EQE curve for $E \approx E_G$. However, the otherwise good accuracy of this approach will become clear later in the article. Although the EQE can be increased by Ag alloying, substantial collection losses are still evident (blue area). The decreasing EQE with increasing wavelength (λ) indicates a poor L_n for both solar cells. Figure 1b displays the corresponding *I–V* curves of the best cells for both samples. While J_{SC} improves, V_{OC} and FF are reduced when the Ag precursor is added, resulting in only a minor efficiency gain from 4.8 to 5.0%. The lower FF and higher J_{SC} are representative for all "pre-Ag" samples. However, the trend of a lower V_{OC} is not as evident for the other runs (see **Figure 2**). Figure 1c,d present scanning electron microscopy (SEM) images of the corresponding solar cells. Similar to low-gap chalcopyrite films,[27] the $CuGaSe_2$ grain size increases when Ag is added as a precursor, in line with earlier findings.[55] This could potentially explain (in parts) the better carrier collection. Still, rather small grains are observed at the interfaces. Especially at the front, the high grain boundary density may facilitate recombination and contribute to the overall poor efficiency.

In the next step, instead of adding Ag as a precursor film, it was coevaporated alongside the other metal elements during absorber growth (keeping a constant Cu/Ag flux ratio). Two different amounts of Ag, AAC = 0.2 and AAC = 0.4, were evaluated. It was deliberately decided to stay below AAC = 0.5 because earlier studies on wide-gap ACIGS indicate (long-term) stability issues and excessive formation of ordered vacancy compounds for AAC > 0.5.[47,60] A potential drawback is that even for the highest value of AAC = 0.4 a detrimental negative CBO of about −0.15 eV is predicted at the interface to CdS,[21] giving rise to increased interface recombination as compared to AAC > 0.5.

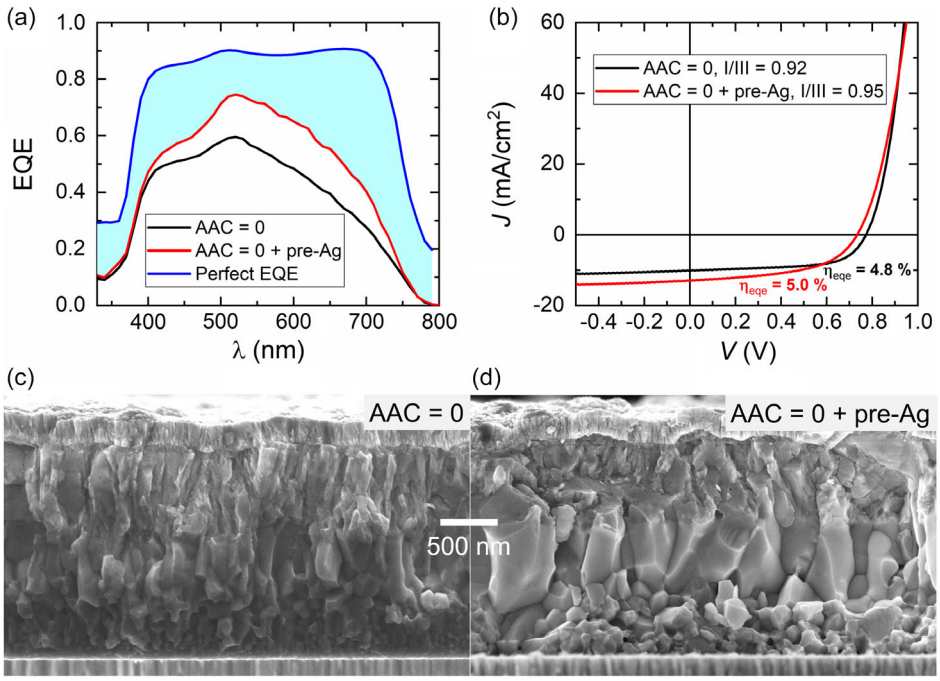

Figure 1. a) EQE spectra of $CuGaSe_2$ samples without and with a 10 nm Ag precursor layer. b) Corresponding *I–V* characteristics. c,d) Corresponding SEM cross-sectional images. Both samples use a CdS buffer.

In addition, the effect of increasing the maximum ACGS deposition temperature from 550 to 600 °C was investigated.

Figure 2 summarizes the best *I–V* parameters (as well as the $J_{SC,eqe}$ values) for all samples as a function of the I/III values. The two different I/III ranges in (a) and (b) were chosen to highlight the overall trend (including highly overstoichiometric absorbers) and the trend toward perfect stoichiometric composition (I/III ≈ 1) separately. To assure the best possible comparability, the light intensity during the *I–V* measurements was calibrated via a Si reference cell for all samples. However, when comparing the corresponding $J_{SC,iv}$ with the values derived from respective EQE measurements ($J_{SC,eqe}$), it is evident that, albeit similar trends, $J_{SC,iv}$ significantly underestimates the cell performance ($J_{SC} \approx 1$–2 mA cm^{-2} lower). This is mainly due to the large mismatch factor of the used light source and the different band gaps of ACGS and Si. Thus, the *I–V* of the best solar cell was remeasured for each sample under a light intensity that results to the $J_{SC,eqe}$ value. Corresponding efficiency values are indicated as η_{eqe} throughout the article (instead of η_{iv} when a Si reference cell was used for calibration).

Let us first consider the effect of absorber stoichiometry on V_{OC}. Independent of the Ag content, the highest V_{OC} values saturate for I/III < 0.90. Higher I/III values result in a monotonous V_{OC} drop toward (and even beyond) the stoichiometric point. On average, V_{OC} is slightly increasing with increasing AAC addition, exceeding 0.8 V for some cells with AAC = 0.4. No clear V_{OC} gain is detected when increasing the ACGS deposition temperature.

By contrast, J_{SC} is monotonously increasing toward stoichiometric absorber composition and a saturation (minimum J_{SC}) may be surmised for I/III < 0.80. This anticorrelation between V_{OC} and J_{SC} was observed for indium-containing ACIGS solar cells with slightly lower E_G (1.4–1.5 eV) before and attributed to an increasing absorber depletion toward I/III = 1.[48,50] Moreover, a distinct trend of increasing J_{SC} with increasing Ag addition (also for "pre-Ag") is found. Higher temperatures seem to improve J_{SC} as well, at least for off-stoichiometric absorbers.

It is harder to make a general statement about the effects of the different parameter variations on the FF. Just concentrating on I/III ≤ 1, it may be concluded that adding Ag to $CuGaSe_2$ leads to a drop in FF. This seems to be most evident when adding it as a precursor. However, most samples with AAC = 0.4 exhibit similar values of about 65% as reached for pure $CuGaSe_2$. So, the relationship is apparently more complex. It is believed that the FF of wide-gap chalcopyrite solar cells is mainly determined by the extent of the voltage-dependent photocurrent collection,[7,48] which depends on the absorber doping and electron diffusion length. A more detailed discussion will be provided below.

Finally, highest efficiencies are measured for the samples with AAC = 0.4 grown at an increased temperature of 600 °C. The *I–V* characteristics of the best cell are plotted in **Figure 3**a together with those of the best cells from all other samples. Overall, the highest efficiency of $\eta_{eqe} = 8.3\%$ ($V_{OC} = 784$ mV, FF = 62.2%, $J_{SC,eqe} = 17.1$ mA cm^{-2}) is reached for a cell with AAC = 0.4 and I/III = 0.88. Figure 3b plots the V_{OC} and $J_{SC,eqe}$ values from Figure 2 against each other. The color code of the data points represents the I/III value of the samples (red: close to stoichiometric, blue: off-stoichiometric). The samples with I/III ≥ 1.10 were excluded and the range of the color code is set to 0.86 < I/III < 1.00 to emphasize the trends. A clear transition from low (<0.7 V) to high (>0.75 V for most samples) V_{OC} values is observed in the range of 1.00 > I/III > 0.92 (color code transitions from red to blue). Moreover, the abovementioned anticorrelation between $J_{SC,eqe}$

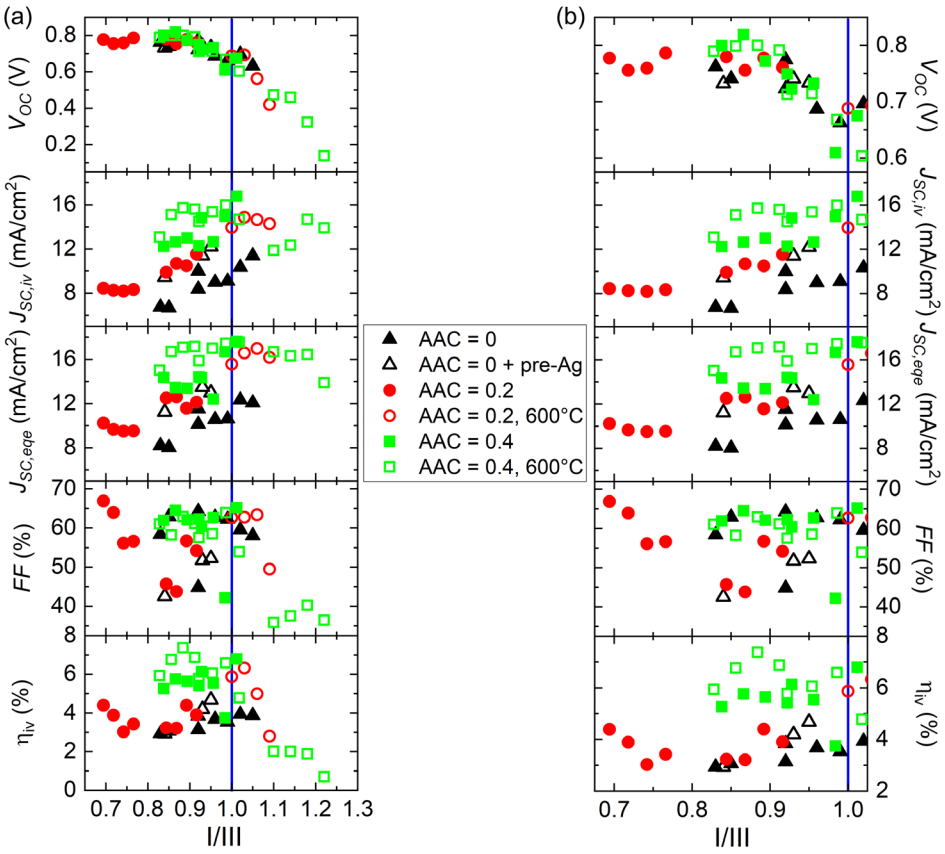

Figure 2. a,b) Best *I–V* parameters and corresponding $J_{SC,eqe}$ values as a function of the I/III values for all samples with CdS buffers. In (a) the entire range in I/III is shown (i.e., all measured samples), while (b) zooms into the region I/III < 1.02 to highlight the trends toward stoichiometric absorber composition.

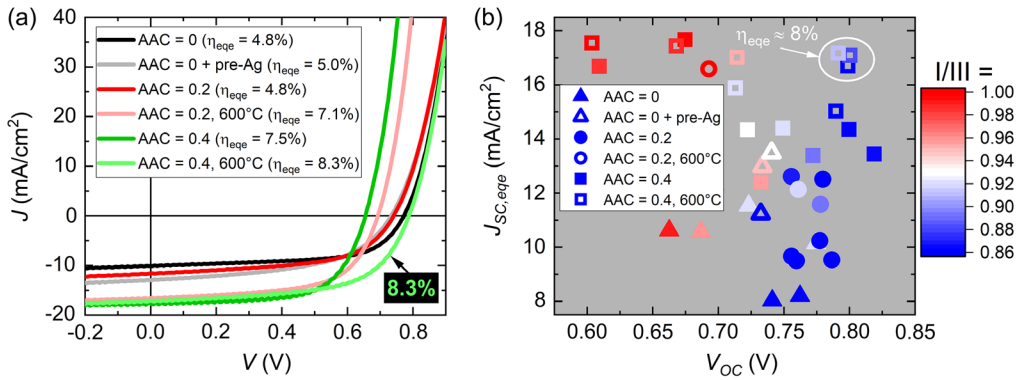

Figure 3. a) *I–V* characteristics of the best cells from each sample (corresponding efficiency values given in legend). b) V_{OC} versus $J_{SC,eqe}$ (same data as in Figure 2) excluding samples with I/III ≥ 1.10. The color code represents the I/III values and the range was set to 0.86 < I/III < 1.00. All samples use CdS as a buffer layer.

and V_{OC} is evident for the majority of samples with AAC ≤ 0.2. However, the solar cells with AAC = 0.4 do not lose as much $J_{SC,eqe}$ when going off-stoichiometric. Increasing the temperature to 600 °C further mitigates collection losses for off-stoichiometric absorber compositions, leading to the highest efficiencies >8%.

Figure 4 shows the EQE spectra of the best solar cells from all samples with I/III ≤ 1.05. Again, the color code represents the corresponding I/III values and the range is set to 0.69 < I/III < 1.05. The "perfect EQE" curve, already shown in Figure 1, is added as well. Some of the samples contained an i-ZnO layer (visible by the slightly higher EQE at low λ), which led to a marginal reduction in $J_{SC,eqe}$. The dashed lines correspond to an energy of 1.64 eV. Obviously, the bandgap is not significantly affected by the absorber stoichiometry, Ag alloying, or

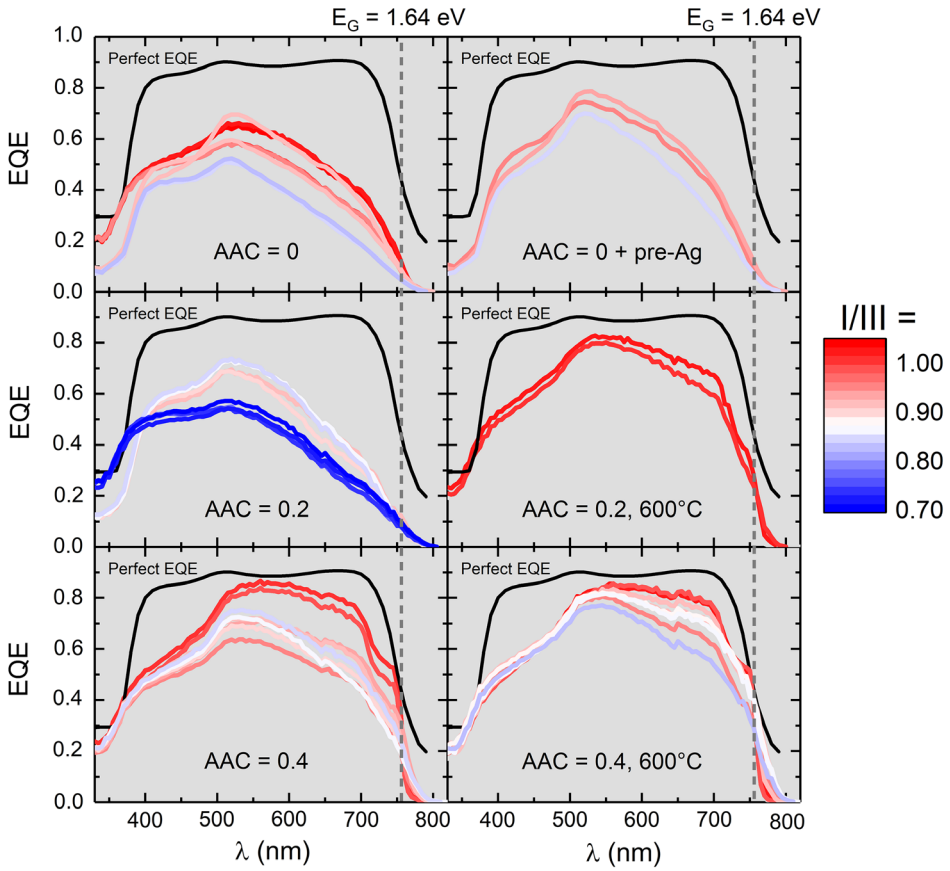

Figure 4. EQE spectra of the best solar cells from all samples with I/III $\leq$ 1.05 (compare corresponding $J_{SC,eqe}$ values in Figure 2). The color code represents the I/III values and ranges from 0.69 to 1.05. All samples use CdS as a buffer.

deposition temperature. Only for AAC = 0.4, a slight reduction to $E_G = 1.62$ eV (from first derivative) is deduced.

It is evident that the carrier collection improves with Ag addition, higher deposition temperature, and toward stoichiometric absorber composition. Highest EQE levels are reached for the samples with I/III close to one. However, the maximum level for those close-stoichiometric samples increases with Ag addition. The best EQE spectra for AAC = 0.4 approach the "perfect EQE" at $\lambda \approx 550$ nm (corresponding to the CdS absorption edge). For longer wavelengths, a small, but non-negligible loss in carrier collection is visible that increases with higher λ. Overall, these results very much resemble our earlier findings for wide-gap ACIGS solar cells with slightly lower E_G of 1.4–1.5 eV. Here, we identified a very low diffusion length ($0\,\text{nm} < L_n < 300\,\text{nm}$) and a significantly decreasing doping density toward stoichiometric absorber composition.[48] This combination results in a strongly voltage- (and composition-) dependent carrier collection.

In order to validate that the same scenario prevails for the ACGS samples in this study, EQE spectra of a "AAC = 0 + pre-Ag" sample (I/III = 0.92) were measured under different voltage biases (V_{bias}) from 0 to −5 in 0.5 V steps. The results are shown in **Figure 5a** together with the "perfect EQE" curve. While the nonbiased cell exhibits distinct carrier collection losses, the EQE continuously approaches the "perfect EQE" with increasing negative V bias. For $V_{bias} = -5$ V, the EQE matches the "perfect EQE" very well for $\lambda > 530$ nm, indicating perfect ("internal") collection. Corresponding capacitance–voltage profiling on the same sample (not shown here) revealed that the absorber is fully depleted (i.e., space charge region width W_{SCR} equals the absorber thickness ($d_{abs} \approx 2\,\mu$m)) for $V_{bias} \leq -4.5$ V and has a nonbiased W_{SCR} of about 450 nm. The fact that a full depletion is necessary to collect all electrons confirms a very low L_n in the ACGS film. Figure 5b illustrates the gains by the V bias as compared to the nonbiased cell. A clear and monotonously improving collection is seen with increasing λ and negative voltage bias. Again, this strongly suggests that the main (if not all) collection occurs inside the space charge region (SCR) and that in the absence of an electric field, the ACGS bulk does not significantly contribute to J_{SC}. The results further indicate that J_{SC} is not limited by interface recombination or internal transport barriers, but exclusively governed by bulk recombination.

The theoretical bias dependence of the EQE for an ACGS solar cell with a very low diffusion length was further derived analytically by using a standard expression for the internal carrier collection efficiency $f_C(x)$,[61] assuming perfect collection in the space charge region. The effect of the bias was approximated by only changing W_{SCR} while keeping the (very low) diffusion length $L_n = 3$ nm (randomly chosen) and the back-contact recombination velocity $S_{bc} = 10^7$ cm s^{-1} constant. The absorption coefficient of the absorber was set to $\alpha_{abs} = 6 \times 10^4 \cdot \sqrt{E - E_G}$ 1 cm^{-1},

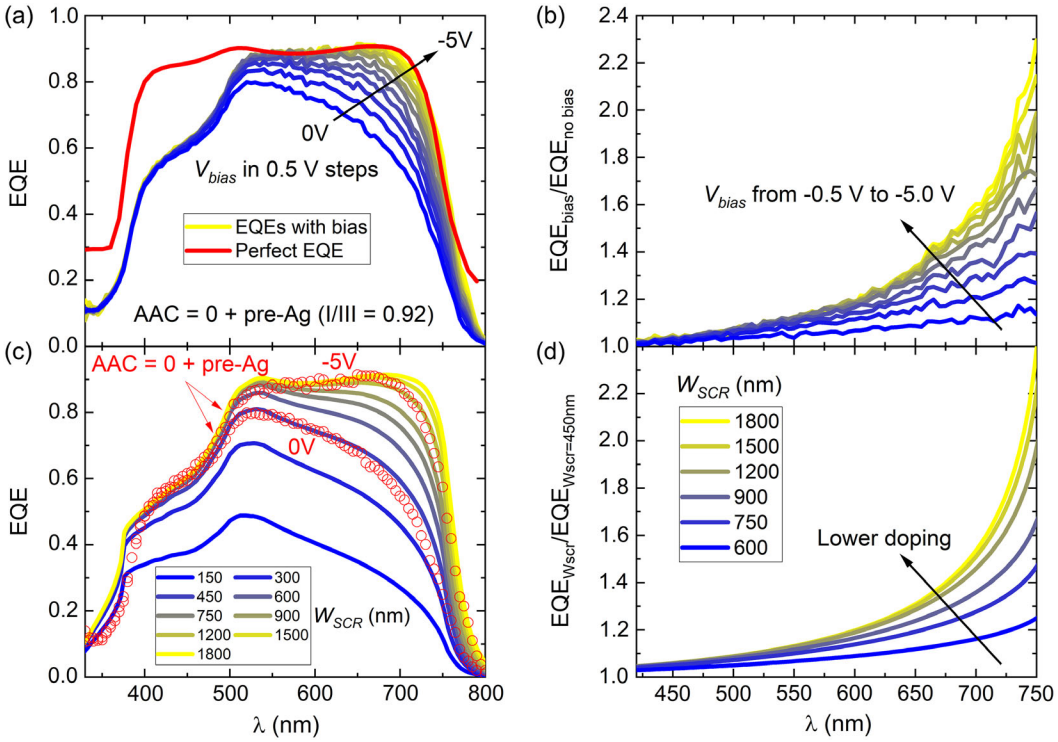

Figure 5. a) EQE spectra of an "AAC = 0 + pre-Ag" sample (I/III = 0.92) measured at different negative bias voltages together with the "perfect EQE" curve. b) Relative EQE gain by applying the different negative voltage biases. c) Calculated EQE spectra for different W_{SCR}, assuming perfect collection in the space charge region and $L_n = 3$ nm. The measured values from (a) for $V_{bias} = 0$ and −5 V are superimposed. d) Corresponding calculated relative EQE gain when increasing W_{SCR} from 450 nm (i.e., W_{SCR} @ 0 V) to different other values.

with $E_G = 1.63$ eV and an absorber thickness of $d_{abs} = 2$ µm. In addition, an Urbach energy of 30 meV was assumed. Figure 5c shows the corresponding spectra for W_{SCR} ranging from 150 to 1800 nm. The measurement data for $V_{bias} = 0$ and −5 V for the "AAC = 0 + pre-Ag" sample from Figure 5a are superimposed. Obviously, the calculated EQE spectra for $W_{SCR} = 450$ nm (i.e., measured value @ $V_{bias} = 0$ V) and $W_{SCR} = 1800$ nm (i.e., roughly the measured value @ $V_{bias} = -5$ V) are very well in line with the experimental results. Figure 5d displays the corresponding theoretical gain in EQE when extending the space charge region beyond 450 nm. The trends are very similar (even quantitatively) to the measured ones in Figure 5b. This further suggests that the assumption of a negligibly small L_n for ACGS is correct. As a consequence, the J_{SC} value of the ACGS solar cells should be essentially determined by the doping (i.e., depletion) of the absorber.

In order to validate this assumption, capacitance–voltage profiling was conducted for each of the samples. The resulting W_{SCR} values are plotted as a function of I/III in **Figure 6**a. The pure $CuGaSe_2$ films exhibit the narrowest space charge region (all < 500 nm). Adding the Ag precursor leads to a slightly larger W_{SCR}. The trend is not so clear for the AAC = 0.2 samples. Here, some very off-stoichiometric samples have a similar depletion width as for AAC = 0, while others show $W_{SCR} > 1$ µm. Adding more silver leads to an even larger W_{SCR} for most of the samples and many do approach full depletion ($W_{SCR} \approx d_{abs}$). Figure 6b illustrates the measured $J_{SC,eqe}$ (see corresponding EQE spectra in Figure 4) in dependence of the deduced W_{SCR} values. The dashed gray line shows the simulated $J_{SC,eqe}$ trend extracted from the calculated EQEs in Figure 5c. The maximum value was adjusted to the highest measured $J_{SC,eqe}$ value. The majority of the data points follow the simulated trend rather nicely, which suggests that the carrier collection is indeed almost exclusively governed by the space charge region for most samples. However, especially the four data points for AAC = 0.2 with $W_{SCR} > 1$ µm deviate significantly from the trend. The origin of this discrepancy is not understood at this point, but could result from changes in electrical properties (e.g., doping) between the dates of EQE and CV characterization (about 8 weeks).

In summary, the measured trends in J_{SC} can be largely ascribed to differences in absorber doping and the resulting variation in W_{SCR}. However, it remains unclear why the higher deposition temperature increases the collection efficiency for off-stoichiometric samples with AAC = 0.4. This may be partly explained by a slightly lower doping, but also a contribution from an improved L_n cannot be ruled out. Indeed, the higher deposition temperature leads to a significant increase in grain size, as can be seen in **Figure 7**. If grain boundaries act as pronounced recombination paths in wide-gap chalcopyrite solar cells, as suggested in ref. [16], larger grains would contribute to the better collection efficiency for off-stoichiometric samples with AAC = 0.4. The anticorrelation between J_{SC} and V_{OC} in the "transition zone" from I/III = 0.9 to 1.0 is presumably caused by a change in absorber doping density. However, this alone cannot

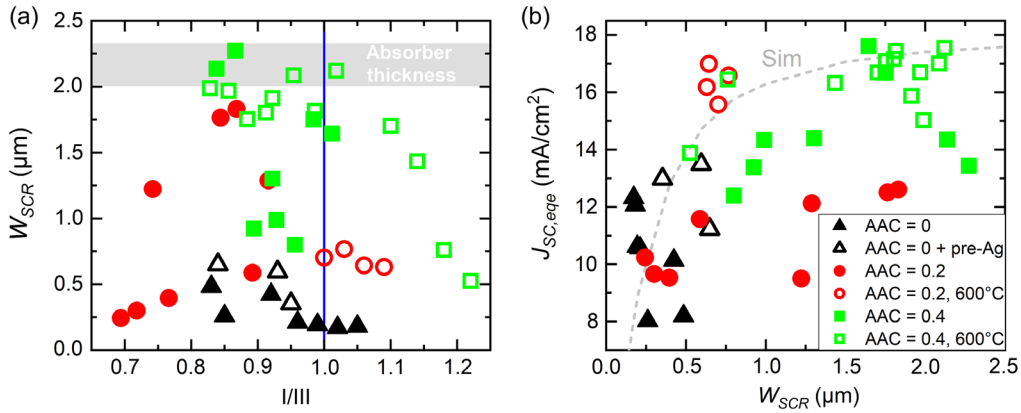

Figure 6. a) Space charge region width as a function of I/III value for all samples, as measured by capacitance–voltage profiling. b) Measured $J_{SC,eqe}$ versus corresponding W_{SCR} values. The dashed line represents the theoretical trend for a cell with a very low L_n of 3 nm, deduced from the calculated EQE spectra in Figure 5c. The legend in (b) is also valid for (a). All samples use CdS as a buffer.

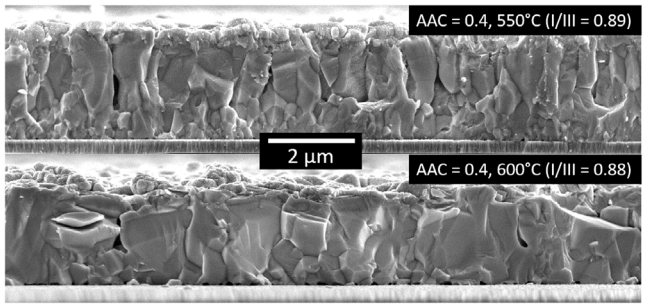

Figure 7. SEM images showing the cross sections of ACGS samples with AAC = 0.4 and different absorber deposition temperatures of 550 and 600 °C, respectively.

explain why the best cells (AAC = 0.4 @ 600 °C) can maintain a relatively high V_{OC}, although they show full depletion/low doping. Thus, it is speculated that the electron lifetime is indeed (at least slightly) improved for higher Ag contents and higher deposition temperatures.

2.2. Replacing the CdS Buffer Layer by $(Zn_{1-y},Sn_y)O_z$

In the second part of this study, the CdS buffer layer was exchanged by a roughly 20 nm thin $(Zn_{1-y},Sn_y)O_z$ film grown via atomic layer deposition (ALD). It was shown before that by reducing the ALD growth temperature or increasing the [Sn]/([Sn]+[Zn]) (Sn/Me) ratio in the film (until at least Sn/Me ≈ 0.24) the electron affinity is monotonously decreasing.[22,57] This allows to avoid, or at least mitigate, a detrimental negative CBO at the absorber/buffer interface, effectively cancelling out interface recombination and improving V_{OC} for $CuGaSe_2$ solar cells to about 1 V.[2] Even on silver containing wide-gap ACIGS devices, the application of the ZTO buffer led to improved efficiencies before.[21] An illustration of the estimated conduction band offsets at the absorber/buffer interface for the investigated ranges in Ag content in the absorber and Sn content in the ZTO buffer is provided in Figure S1, Supporting Information. In addition, the higher bandgap ($E_G > 3.3$ eV) reduces the parasitic absorption of high-energy photons and thereby the relative increase in J_{SC} is higher than for corresponding low-gap CIGS and ACIGS solar cells.

As the cells with CdS buffers showed a clear improvement in performance with increasing ACGS deposition temperature, it was further increased to 650 °C for all samples with a ZTO buffer. Three different absorber deposition runs were conducted with AAC = 0.15, 0.35, and 0.40 in the stoichiometry range of 0.87 < I/III < 1.00. The samples from the first two runs with AAC = 0.15 and 0.35 were cut in half and ZTO buffers with two different Sn/Me ratios of 0.21 and 0.28 were deposited on top. In this way, the effect of the Sn/Me ratio can be directly evaluated for cells with very similar ACGS composition.

The results from *I–V* characterization (best values only) are summarized in **Figure 8**. For a better comparison, the data of the CdS-buffered cells (see Figure 2) are added in gray. The most striking effect when replacing CdS by ZTO is the higher V_{OC}. In stark contrast to samples with CdS, the cells with ZTO seem to show increasing V_{OC} values toward stoichiometric ACGS composition, with V_{OC} up to 974 mV for a cell with AAC = 0.35 and Sn/Me = 0.28. However, no clear V_{OC} trend with varying Ag content and ZTO composition is visible. This may indicate that interface recombination is effectively cancelled out for all samples (except for the one with AAC = 0.35 and Sn/Me = 0.21; not understood at this point) and the remaining V_{OC} deficit is exclusively caused by the poor bulk quality. The application of the ZTO buffer further leads to higher $J_{SC,eqe}$ values, with about 19 mA cm^{-2} for the best close-stoichiometric samples, mainly due to the lower parasitic absorption. The FF is higher for samples with Sn/Me = 0.21 as compared to Sn/Me = 0.28, indicating that the conduction band minimum (CBM) is further lifted when going to Sn/Me = 0.28, which may form a (slightly) too large electron barrier at the ZTO/ACGS interface. The samples with AAC = 0.40 and Sn/Me = 0.26 show an increasing FF with increasing I/III. However, even for the highest I/III of 0.97, the cells still show lower FF values as compared to the other samples with lower AAC. This may be caused by a combination of the highest AAC (leading to lowest conduction band level of absorber)

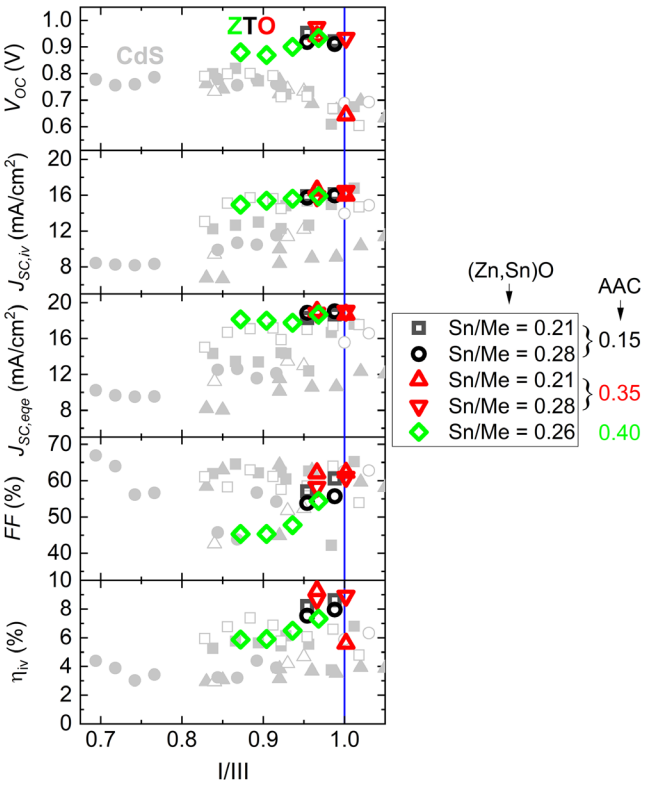

Figure 8. Best *I–V* parameters and corresponding $J_{SC,eqe}$ values as a function of the I/III values for all samples with ZTO buffer layers. The data for samples with CdS buffers (see Figure 2) are added in gray.

and a quite high Sn/Me. Overall, the highest efficiencies are reached for samples with AAC = 0.35.

For the best cells, the *I–V* was again remeasured with adjusted (i.e., increased) light intensity to match the $J_{SC,eqe}$ values. **Figure 9**a shows the results together with the *I–V* curve of the best cell with CdS from the previous section of the paper (legend in Figure 9b). The highest efficiency value of $\eta_{eqe} = 11.0\%$ was measured for the cell with AAC = 0.35, I/III = 0.97, and Sn/Me = 0.21. Increasing the Sn/Me to 0.28 for the same absorber leads to a higher V_{OC} (989 mV), but a significantly lower FF. The samples with AAC = 0.40 showed the lowest efficiency, potentially due to an electron transport barrier at the heterojunction. Indeed, according to the CBM positions sketched in Figure S1, Supporting Information, a positive CBO of about 130 meV is estimated at the ZTO/ACGS interface for this sample. Assuming a very low ZTO doping (i.e., strong voltage-drop in the buffer), this CBO value may be sufficient to impede the electron transport (i.e., large barrier for thermionic emission) across the heterojunction. The corresponding EQE spectra are illustrated in Figure 9b. The large gain in EQE for $\lambda < 530$ nm, caused by the higher E_G of the ZTO buffer, is clearly visible. Otherwise, the EQE spectra of all samples are rather similar. For the sample with AAC = 0.40, a MgF_2 ARC was deposited later. The corresponding EQE is added as well.

It was found that the performance of chalcopyrite solar cells with ZTO buffers can be improved/restored after a light soaking (LS) treatment.[62] In order to test a similar beneficial effect for samples in this study, the cells shown in Figure 9a were exposed to white light (≈30 mW cm^{-2}) for 24 h without actively cooling the cells (i.e., they heat up to about 45 °C). As can be seen in **Figure 10**a, albeit the kink in the *I–V* curves (indicating an electron barrier) is somewhat attenuated, the LS did not have a significant effect on the efficiency of the cells with AAC = 0.35 (similar behavior for samples with AAC = 0.15). However, the sample with AAC = 0.40 and Sn/Me = 0.26 clearly improved after LS (see Figure 10b). The efficiency increased from $\eta_{eqe} = 8.5\%$ to 11.2% by a large increase in FF to 61.0% and in V_{OC} to 985 mV ($J_{SC} = 18.6$ mA cm^{-2}). This is the highest efficiency ever measured on a (A)CGS solar cell without an ARC. Possible explanations for the beneficial effect of the LS may be the photodoping of the ZTO layer that would reduce the effective barrier height for electrons, or a redistribution of sodium at the heterojunction. In order to increase the efficiency, a MgF_2 ARC was deposited on this sample, four weeks after the initial measurement (see EQE in Figure 9b). The reduced cell reflection increased $J_{SC,eqe}$ from 18.6 to 20.6 mA cm^{-2}. Unfortunately, the FF and V_{OC} slightly degraded to 58.0% and 973 mV, respectively, after the storage period in a nitrogen-containing atmosphere, resulting in an efficiency of $\eta_{eqe} = 11.6\%$. This value is slightly below the world record of 11.9% for pure $CuGaSe_2$.[2]

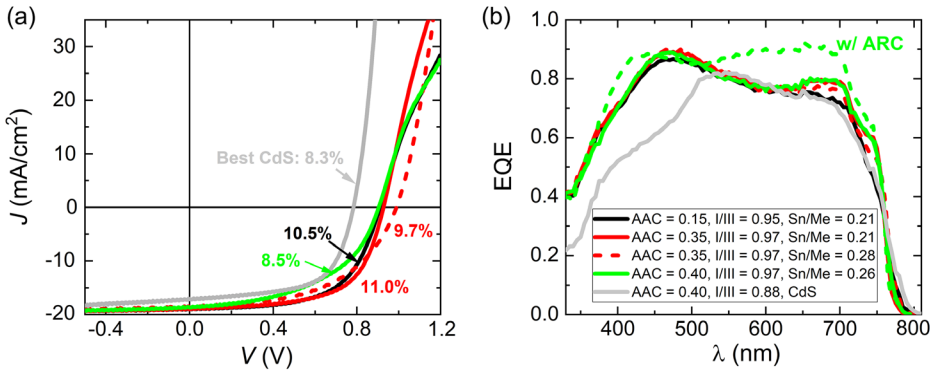

Figure 9. a) *I–V* characteristics of the best cells from selected samples with different compositions of the ZTO buffer (legend can be found in (b)). The efficiency values (η_{eqe}) are indicated at the respective curves and the *I–V* of the best cells with CdS (deposition temperature of 600 °C) is added as well. b) Corresponding EQE spectra. For the sample with AAC = 0.40 and Sn/Me = 0.26 an ARC was deposited subsequently. The corresponding EQE is shown, too.

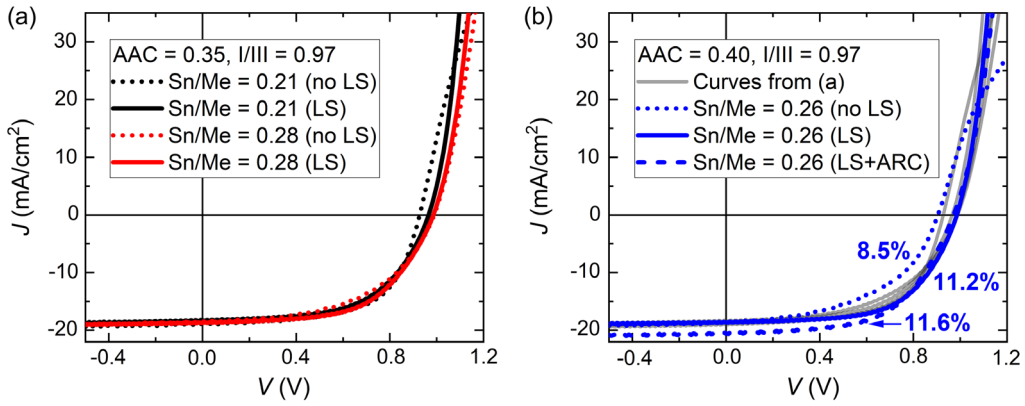

Figure 10. a) *I–V* characteristic of the best ACGS cells with AAC = 0.35, I/III = 0.97, and two different ZTO buffer compositions before and after 24 h LS. b) *I–V* characteristics of the best ACGS cell with AAC = 0.40, I/III = 0.97, and Sn/Me = 0.26 before and after 24 h LS as well as after ARC deposition. The *I–V* curves from (a) are added in (b) for direct comparison.

The next steps on the way to make a wide-gap ACGS top cell for application in a tandem device are to improve the long-term stability (e.g., by choosing thicker ZTO[62]) and to use TBCs (like In_2O_3:Sn or In_2O_3:H[28,30,31]) instead of a Mo back contact. This will bring new challenges like the detrimental formation of GaO_x at the back contact.[23,28] In order to mitigate GaO_x formation, the sodium supply needs to be accurately tailored, especially when increasing the absorber deposition temperatures > 550 °C to improve the ACGS properties.[28,63] Ultimately, to make (A)CGS a true option for a top cell in a tandem device and competitive compared to other candidates like perovskites, the bulk quality (i.e., electron lifetime) needs to be significantly improved. While silver alloying mainly improves the minority carrier collection by widening the space charge region, it does not increase the electron lifetime enough to avoid 1) significant V_{OC} losses (>350 mV, cf., radiative limit even with ZTO buffer), 2) J_{SC} losses for off-stoichiometric absorbers, and 3) low FF values (typically <70%) originating from the strongly *V*-dependent collection. Thus, Ag alloying is not the silver bullet that closes the long-standing efficiency gap between low- and wide-gap chalcopyrite solar cells. Increasing the lifetime in ACGS is not an easy task and different approaches such as defect passivation by extrinsic elements should be (re-)evaluated.[64–66]

3. Conclusions

This study evaluates the potential of combining the application of alternative (Zn,Sn)O buffer layers with a tailored silver alloying to improve the performance of $CuGaSe_2$-based solar cells. The first part of the work focuses on the effect of the Ag content, absorber stoichiometry, and growth temperature in CdS-buffered devices. It is found that silver addition mainly increases J_{SC} by decreasing the absorber doping. The results clearly suggest a very low diffusion length, leading to negligible carrier collection outside the SCR. A small increase in V_{OC} with increasing AAC may be attributed to the lower conduction band misalignment at the CdS/ACGS interface, the increase in grain size, and/or a favorable energy shift of deep defect levels (e.g., Ga_I). Increasing the deposition temperature leads to a further ACGS grain enlargement. The highest efficiency for a CdS-buffered cell of 8.3% is reached for a cell with AAC = 0.4 processed at 600 °C. Overall, a strong impact of the absorber stoichiometry on device performance is evident. A distinct anticorrelation between J_{SC} and V_{OC} is observed in the range of 0.9 < I/III < 1.0, with decreasing V_{OC} values toward stoichiometric composition. It is proposed that this is mainly an effect of the change in doping, but other mechanisms cannot be ruled out.

This anticorrelation is not observed when using a ZTO buffer, showing the highest V_{OC} (approaching 1 V) and J_{SC} values for close-stoichiometric absorbers. At this point it is not understood why the trend with varying I/III is so different when changing from CdS to ZTO. The large improvement in V_{OC} is mainly caused by reducing (or cancelling out) interface recombination. Light soaking increases the FF for most of the samples, potentially by mitigating internal transport barriers. The best cell with AAC = 0.40 (deposition temperature of 650 °C) and a ZTO composition of Sn/Me = 0.26 reaches an efficiency of 11.2% (no ARC) after LS. This is the highest efficiency ever measured on a (A)CGS solar cell without an ARC. The 4 weeks storage time in a N_2-cabinet until deposition of an ARC led to a slight parameter degradation and thus, only a minor efficiency gain (11.6% w/ARC).

4. Experimental Section

Solar Cell Processing: The solar cells processed in this study are stacked in the sequence: glass substrate/Mo/NaF-precursor/(A)CGS/CdS or ZTO/(i-ZnO)/ZnO:Al. The glass substrate was standard soda-lime glass (SLG) for most absorber depositions at 550 °C and for higher temperatures high strain point glass, with a higher K content ("PV200") was always used. Some of the samples deposited at 550 °C also had PV200 as a substrate, but no clear effect of the glass type on the device performance was detected between samples with otherwise similar deposition conditions. However, it shall be mentioned here that in-diffusion of potassium and its agglomeration at the buffer interface was found in glow-discharge optical emission spectroscopy (GDOES) measurements for samples with PV200 substrates (not shown here). First, the 320 nm-thick Mo back contact was sputter-deposited and then coated with a 15 nm-thick NaF precursor layer. No alkali diffusion barrier was introduced underneath the back contact.

A three-stage (I-poor → I-rich → I-poor) coevaporation process was applied to grow 2.0–2.3 µm-thick (A)CGS films at a maximum temperature

of 550 or 600 °C for the CdS-buffered samples and 650 °C for the ZTO-buffered ones. Silver was added in a way that the ratio of the Ag and Cu evaporation rates was kept constant at any time. This absorber deposition protocol led to homogenous elemental depth profiles (i.e., no gradients), as confirmed by GDOES measurements (not shown here). A heavy alkali postdeposition treatment was not implemented. In total, 12 (A)CGS deposition runs were done that got CdS buffers (first part) and three that used ZTO as a buffer (second part). This resulted in a large set of samples with different AAC (= 0–0.4) and I/III (= 0.69–1.22) values. Differences in composition emanate from the lateral distribution of the metal sources in the evaporation chamber. For additional information about the metal evaporation rate sequences and source configuration, we refer to the supporting information in ref. [48].

After absorber deposition, either an ≈55 nm-thick CdS buffer layer was grown via CBD at 60 °C or an ≈20 nm-thick ZTO layer was deposited by ALD in an F-120 reactor (ASM Microchemistry) at a temperature of 120 °C. For the ALD process, diethylzinc [DEZ or $Zn(C_2H_5)_2$], tetrakis(dimethylamino) tin(IV) [TDMASn or $Sn(N(CH_3)_2)_4$], and deionized water were used as precursors and N_2 as a carrier/purge gas. The Zn/Sn:N_2:H_2O:N_2 pulse times were set to 400:800:400:800 ms, respectively, and 700 cycles were grown in a supercycle scheme. The Zn:Sn pulse ratios were varied to change the composition of the ZTO films. The corresponding 2:3, 3:4, and 5:6 ratios led to Sn/Me values of 0.28, 0.26, and 0.21, respectively, in the final films.

Finally, a 200 nm-thick ZnO:Al layer was sputtered on top. Some of the CdS-buffered samples processed in the very beginning of this experimental series also contain a 60 nm-thick i-ZnO layer between the buffer and the ZnO:Al (visible in EQE spectra in Figure 4). However, it was found that skipping i-ZnO is not detrimental for the device performance of the ACGS devices and thus, it was omitted for the majority of the samples. All cells with ZTO do not have an i-ZnO layer. The completed samples were sectioned into 14 individual solar cells ($A = 0.05$ cm^2) via mechanical scribing.

Material Characterization: Integral (A)CGS absorber and ZTO buffer compositions were determined with a Panalytical Epsilon 5 XRF spectrometer. Optical characterization (R & T measurements) of SLG/ACGS and full cell stacks was conducted in a Perkin Elmer Lambda 900 spectrometer with an integrating sphere. A Zeiss Merlin SEM (acceleration voltage of 5 kV) was used to investigate the solar cell cross sections.

Electro-Optical Characterization of Solar Cells: The *I–V* (all 14 cells per sample) and EQE (only best cell each) measurements of completed solar cells were done using home-built setups. The *I–V* characteristics were measured at $T = 25$ °C under illumination by an ELH lamp. For each sample, the light intensity was adjusted to match the J_{SC} value of a calibrated Si reference solar cell. After measuring *I–V* on all solar cells, the EQE was measured only on the best cells for each sample. Due to the difference in E_G between the Si reference cell and the investigated absorbers, the strong deviation of the ELH lamp spectrum from the AM1.5 G spectrum leads to a large mismatch factor. To correct for that, the *I–V* of the best cells were remeasured subsequently at an increased light intensity, matching the $J_{SC,eqe}$ values derived from the corresponding EQE spectra. Capacitance–voltage profiling was conducted from $V = -0.1$ to $+0.1$ V at 100 kHz and an amplitude of 25 mV, using an Agilent 4284 A precision LCR meter and a Keithley 2401 source meter. A dielectric constant of $\varepsilon_r = 10$ was assumed for the ACGS material in this study.

Supporting Information

Supporting Information is available from the Wiley Online Library or from the author.

Acknowledgements

This work was financially supported by the European Union program HORIZON (Call: HORIZON-CL5-2021-D3-02, Project ID: 101075626 (SITA)) and the Swedish Energy Agency under the project number P50992-1, Dnr 2020-009335.

Conflict of Interest

The authors declare no conflict of interest.

Data Availability Statement

Research data are not shared.

Keywords

CIGS, $CuGaSe_2$, silver alloying, tandem devices, wide-gap solar cells

Received: March 17, 2023
Revised: April 13, 2023
Published online: May 4, 2023

[1] M. Alonso, K. Wakita, J. Pascual, M. Garriga, N. Yamamoto, *Phys. Rev. B.* **2001**, *63*, 075203.
[2] F. Larsson, N. S. Nilsson, J. Keller, C. Frisk, V. Kosyak, M. Edoff, T. Törndahl, *Prog. Photovolt. Res. Appl.* **2017**, *25*, 755.
[3] S. Chichibu, T. Mizutani, K. Murakami, T. Shioda, T. Kurafuji, H. Nakanishi, S. Niki, P. J. Fons, A. Yamada, *J. Appl. Phys.* **1998**, *83*, 3678.
[4] A. S. Brown, M. A. Green, *Phys. E.* **2002**, *14*, 96.
[5] R. K. Kothandaraman, Y. Jiang, T. Feurer, A. N. Tiwari, F. Fu, *Small Methods* **2020**, *4*, 2000395.
[6] S. Siebentritt, U. Rau, in *Wide-Gap Chalcopyrites*, Springer-Verlag, Berlin Heidelberg **2006**.
[7] S. Hegedus, W. N. Shafarman, *Prog. Photovolt. Res. Appl.* **2004**, *12*, 155.
[8] B. Huang, S. Chen, H. Deng, L. Wang, M. A. Contreras, R. Noufi, S.-H. Wei, *IEEE J. Photovoltaics.* **2014**, *4*, 477.
[9] J. Pohl, K. Albe, *Phys. Rev. B.* **2013**, *87*, 245203.
[10] C. Spindler, F. Babbe, M. H. Wolter, F. Ehre, K. Santosh, P. Hilgert, F. Werner, S. Siebentritt, *Phys. Rev. Mater.* **2019**, *3*, 090302.
[11] C. Spindler, D. Regesch, S. Siebentritt, *Appl. Phys. Lett.* **2016**, *109*, 032105.
[12] S. Lany, A. Zunger, *J. Appl. Phys.* **2006**, *100*, 113725.
[13] G. Hanna, A. Jasenek, U. Rau, H. W. Schock, *Thin Solid Films.* **2001**, *387*, 71.
[14] G. Hanna, A. Jasenek, U. Rau, H. W. Schock, *Phys. Status Solidi A.* **2000**, *179*, 7.
[15] M. R. Balboul, H. W. Schock, S. A. Fayak, A. A. El-Aal, J. H. Werner, A. A. Ramadan, *Appl. Phys. A.* **2008**, *92*, 557.
[16] M. Raghuwanshi, E. Cadel, P. Pareige, S. Duguay, F. Couzinie-Devy, L. Arzel, N. Barreau, *Appl. Phys. Lett.* **2014**, *105*, 013902.
[17] S.-H. Wei, A. Zunger, *J. Appl. Phys.* **1995**, *78*, 3846.
[18] M. Gloeckler, J. R. Sites, *Thin Solid Films.* **2005**, *480–481*, 241.
[19] M. Turcu, O. Pakma, U. Rau, *Appl. Phys. Lett.* **2002**, *80*, 2598.
[20] S. Ishizuka, *Phys. Status Solidi A.* **2019**, *216*, 1800873.
[21] J. Keller, K. V. Sopiha, O. Stolt, L. Stolt, C. Persson, J. J. S. Scragg, T. Törndahl, M. Edoff, *Prog. Photovolt. Res. Appl.* **2020**, *28*, 237.
[22] J. Lindahl, J. Keller, O. Donzel-Gargand, P. Szaniawski, M. Edoff, T. Törndahl, *Sol. Energy Mater. Sol. Cells.* **2016**, *144*, 684.
[23] T. Nakada, Y. Hirabayashi, T. Tokado, D. Ohmori, T. Mise, *Sol. Energy.* **2004**, *77*, 739.
[24] R. Caballero, S. Siebentritt, K. Sakurai, C. A. Kaufmann, M. C. Lux-Steiner, in *Conf. Rec. 2006 IEEE 4th World Conf. Photovolt. Energy Conversion, WCPEC-4*. IEEE, Piscataway, NJ **2006**, p. 479.
[25] J. H. Choi, K. Kim, Y. J. Eo, J. H. Park, J. Gwak, S. K. Ahn, A. Cho, S. Ahn, J. S. Cho, K. Shin, K. Yoon, S. H. Kong, J. Yoo, *Vacuum.* **2015**, *120*, 42.

[26] A. Thomere, M. Placidi, M. Guc, K. Tiwari, R. Fonoll-Rubio, V. Izquierdo-Roca, A. Perez-Rodriguez, Z. J. Li-Kao, *Prog. Photovolt. Res. Appl.* **2023**, *31*, 524.
[27] S. C. Yang, T. Y. Lin, M. Ochoa, H. Lai, R. Kothandaraman, F. Fu, A. N. Tiwari, R. Carron, *Nat. Energy.* **2022**, *8*, 40.
[28] J. Keller, L. Stolt, O. Donzel-Gargand, T. Kubart, M. Edoff, *Sol. RRL.* **2022**, *6*, 2200401.
[29] M. J. Shin, S. Park, A. Lee, S. J. Park, A. Cho, K. Kim, S. K. Ahn, J. Hyung Park, J. Yoo, D. Shin, I. Jeong, J. H. Yun, J. Gwak, J. S. Cho, *Appl. Surf. Sci.* **2021**, *535*, 147732.
[30] J. Keller, N. Shariati Nilsson, A. Aijaz, L. Riekehr, T. Kubart, M. Edoff, T. Törndahl, *Prog. Photovolt. Res. Appl.* **2018**, *26*, 159.
[31] J. Keller, W.-C. Chen, L. Riekehr, T. Kubart, T. Törndahl, M. Edoff, *Prog. Photovolt. Res. Appl.* **2018**, *26*, 846.
[32] Y. Li, G. Yin, M. Schmid, *Sol. Energy Mater. Sol. Cells.* **2022**, *234*, 111431.
[33] A. Jeong, J. M. Choi, H.-J. Lee, G.-Y. Kim, J.-K. Park, W. M. Kim, S. Kuk, Z. Wang, D. J. Hwang, H. Yu, J. Jeong, *Prog. Photovolt. Res. Appl.* **2022**, *30*, 713.
[34] D. L. Young, J. Keane, A. Duda, J. A. M. A. Shama, C. L. Perkins, M. Romero, R. Noufi, *Prog. Photovolt. Res. Appl.* **2003**, *11*, 535.
[35] M. Saad, H. Riazi, E. Bucher, M. C. Lux-steiner, *Appl. Phys. A.* **1996**, *62*, 181.
[36] R. Caballero, S. Siebentritt, C. A. Kaufmann, C. Kelch, D. Schweigert, T. Unold, M. Rusu, H. Schock, M. C. Lux-steiner, *Mater. Res. Soc. Symp. Proc. 2007*, *1012*, 1012-Y12-38.
[37] S. Ishizuka, R. Okamoto, S. Ikeda, *Adv. Mater. Interfaces.* **2022**, *9*, 2201266.
[38] F. Khavari, J. Keller, J. K. Larsen, K. V. Sopiha, T. Törndahl, M. Edoff, *Phys. Status Solidi A.* **2020**, *217*, 2000415.
[39] A. Hultqvist, C. Platzer-Björkman, J. Pettersson, T. Törndahl, M. Edoff, *Thin Solid Films.* **2009**, *517*, 2305.
[40] J. Gong, D. Gao, Z. Ma, X. Yang, J. Zhang, X. Liu, C. Chen, J. Tang, B. Da, J. Li, G. Fang, X. Xiao, *Sol. RRL.* **2022**, *2200766*, 2200766.
[41] A. Chirila, P. Reinhard, F. Pianezzi, P. Blösch, A. R. Uhl, C. Fella, L. Kranz, D. Keller, C. Gretener, H. Hagendorfer, D. Jaeger, R. Erni, S. Nishiwaki, S. Buecheler, A. N. Tiwari, *Nat. Mater.* **2013**, *12*, 1107.
[42] S. Chen, X. G. Gong, S. H. Wei, *Phys. Rev. B.* **2007**, *75*, 205209.
[43] D. Huang, J. W. Jiang, J. Guo, Y. J. Zhao, R. Chen, C. Persson, *Mater. Sci. Eng. B.* **2018**, *236–237*, 147.
[44] G. M. Hanket, J. H. Boyle, W. N. Shafarman, *34th IEEE Photovolt. Spec. Conf.* **2009**, 001240.
[45] T. Nakada, K. Yamada, R. Arai, H. Ishizaki, N. Yamada, *MRS Proc.* **2005**, *865*, F11.1.
[46] T. Umehara, F. Zulkifly, K. Nakada, A. Yamada, *Jpn. J. Appl. Phys.* **2017**, *56*, 08MC09.
[47] J. Keller, L. Stolt, K. V. Sopiha, J. K. Larsen, L. Riekehr, M. Edoff, *Sol. RRL.* **2020**, *4*, 2000508.
[48] J. Keller, P. Pearson, N. Shariati Nilsson, O. Stolt, L. Stolt, M. Edoff, *Sol. RRL.* **2021**, *5*, 2100403.
[49] J. K. Larsen, O. Donzel-Gargand, K. V. Sopiha, J. Keller, K. Lindgren, C. Platzer-Björkman, M. Edoff, *ACS Appl. Energy Mater.* **2021**, *4*, 1805.
[50] J. Keller, H. Aboulfadl, L. Stolt, O. Donzel-Gargand, M. Edoff, *Sol. RRL.* **2022**, *6*, 2200044.
[51] K. Kim, S. K. Ahn, J. H. Choi, J. Yoo, Y. J. Eo, J. S. Cho, A. Cho, J. Gwak, S. Song, D. H. Cho, Y. D. Chung, J. H. Yun, *Nano Energy* **2018**, *48*, 345.
[52] S. Soltanmohammad, H. M. Tong, T. J. Anderson, W. N. Shafarman, *IEEE J. Photovoltaics* **2019**, *9*, 898.
[53] R. Carron, S. Nishiwaki, E. Shih, C. Yang, M. Ochoa, X. Sun, Th. Feurer, A. Tiwari, *NPJ Electron.* **2022**, https://doi.org/10.21203/rs.3.rs-2116168/v1.
[54] S. C. Yang, J. Sastre, M. Krause, X. Sun, R. Hertwig, M. Ochoa, A. N. Tiwari, R. Carron, *Sol. RRL.* **2021**, *5*, 2100108.
[55] T. Nishimura, A. Doi, J. Chantana, A. Mavlonov, Y. Kawano, T. Minemoto, *Sol. Energy.* **2021**, *230*, 509.
[56] A. Hultqvist, M. Edoff, T. Törndahl, *Prog. Photovolt. Res. Appl.* **2011**, *19*, 478.
[57] M. Kapilashrami, C. X. Kronawitter, T. Törndahl, J. Lindahl, A. Hultqvist, W.-C. Wang, C.-L. Chang, S. S. Mao, J. Guo, *Phys. Chem. Chem. Phys.* **2012**, *14*, 10154.
[58] W. Liu, Y. Zhang, Z. Hu, S. Lin, S. Cheng, Z. He, C. Wang, Z. Zhou, Y. Sun, *ACS Appl. Energy Mater.* **2020**, *3*, 9963.
[59] K. Kim, J. W. Park, J. S. Yoo, J. S. Cho, H. D. Lee, J. H. Yun, *Sol. Energy Mater. Sol. Cells.* **2016**, *146*, 114.
[60] P. Pearson, J. Keller, L. Stolt, M. Edoff, C. Platzer Björkman, *Phys. Status Solidi Basic Res.* **2022**, *259*, 2200104.
[61] M. A. Green, *Prog. Photovolt. Res. Appl.* **2009**, *17*, 57.
[62] A. Hultqvist, C. Platzer-björkman, U. Zimmermann, M. Edoff, T. Törndahl, *Prog. Photovolt. Res. Appl.* **2012**, *20*, 883.
[63] M. D. Heinemann, V. Efimova, R. Klenk, B. Hoepfner, M. Wollgarten, T. Unold, H. Schock, C. A. Kaufmann, *Prog. Photovolt. Res. Appl.* **2015**, *23*, 1228.
[64] V. Koteski, S. Doka-Yamigno, J. Hofstetter, M. Rusu, H. E. Mahnke, M. C. Lux-Steiner, T. Schedel-Niedrig, E. Arushanov, *Phys. Rev. B - Condens. Matter Mater. Phys.* **2010**, *81*, 245213.
[65] Ç. Kılıç, A. Zunger, *Phys. Rev. B - Condens. Matter Mater. Phys.* **2003**, *68*, 752011.
[66] M. Han, P. Deák, Z. Zeng, T. Frauenheim, *Phys. Rev. Appl.* **2021**, *15*, 044021.